Experimental evidence of orbital order in α-B_{12} and γ-B_{28} polymorphs of elemental boron

Swastik Mondal, Sander van Smaalen,* Gleb Parakhonskiy, Siriyara Jagannatha Prathapa, Leila Noohinejad, Elena Bykova, and Natalia Dubrovinskaia
Laboratory of Crystallography, University of Bayreuth, D-95440 Bayreuth, Germany

Dmitry Chernyshov
Swiss-Norwegian Beam Line, ESRF, 38043 Grenoble, France

Leonid Dubrovinsky
Bayerisches Geoinstitut, University of Bayreuth, D-95440 Bayreuth, Germany
(Received 3 September 2012; revised manuscript received 11 June 2013; published 29 July 2013)

The electron density of the α form of boron has been obtained by multipole refinement against high-resolution, single-crystal x-ray diffraction data measured on a high-quality single crystal at a temperature of 100 K. Topological properties of this density have been used to show that all chemical bonds between B_{12} clusters in α-B_{12} are formed due to one orbital on each boron atom that is oriented perpendicular to the surface of the cluster. It is shown that the same orbital order on B_{12} clusters persists in both α-B_{12} and γ-B_{28} polymorphs and in several dodecaboranes, despite the fact that in every case the B_{12} clusters participate in entirely different kinds of exocluster bonds. It is likely that the same orbital order of B_{12} clusters can explain bonding in other boron polymorphs and boron-rich solids.

DOI: 10.1103/PhysRevB.88.024118 PACS number(s): 61.50.Ks, 61.05.cp, 61.50.Ah, 61.66.Bi

I. INTRODUCTION

Polymorphs of elemental boron are of wide scientific interest due to their enigmatic physical and chemical properties and bonding.[1–3] A comprehensive description of chemical bonding between boron atoms is of fundamental importance in physics. It may lead to the understanding of the exceptional properties of several boron polymorphs and borides[1]—such as superhardness, low compressibility, and superconductivity—that may help in developing boron-based materials with enhanced properties. Peculiarities in chemical bonding of the high-pressure, high-temperature γ-B_{28} polymorph of boron have been proposed,[2,4] and recently been explained by an experimental electron-density study.[5] An unusual electron-density distribution and bonding has also been suggested for α-B_{12},[6,7] the simplest of all boron polymorphs. Electron-density distributions and bonding mechanisms in other polymorphs of boron are yet to be explored.[1]

The ubiquitous building block of all polymorphs of boron is a twelve-atom cluster (B_{12}) with approximate icosahedral symmetry. Covalent bonding between B_{12} clusters in boron can take place either by direct bonding or via additional atoms. Theoretical calculations[8–10] have shown that the icosahedral B_{12} cluster possesses thirteen internal and twelve external bonding orbitals. According to the Wade-Jemmis rule,[11–13] 26 out of 36 valence electrons of a B_{12} cluster are accommodated in 13 molecular-orbital-like bonding orbitals to form the cluster. This leaves 10 electrons for external bonding using 12 equivalent external bonding orbitals, thus creating an electron deficiency in the cluster. Nature has solved the discrepancy between the number of available valence electrons and the number of bonding orbitals by forming a large variety of two-electron–three-center (2e3c) and one-electron–two-center (1e2c) bonds in combination with the "normal" two-electron–two-center (2e2c) bonds in polymorphs of boron and boron-rich compounds.[1,5,14–18] Maybe it is this large variety of bond types rather than the electron deficient nature itself which makes chemical bonding of boron difficult to understand. The electron-density distribution as determined by x-ray diffraction can provide an experimental picture of the bonding situation.

Recently, on the basis of an experimental electron-density study, we have characterized all bonds in the high-pressure polymorph γ-B_{28},[5] which included a strong 2e2c intercluster bond, a weaker 1e2c intercluster bond, two 2e2c bonds involving additional atoms as well as a unique polar-covalent 2e3c bond comprising two atoms of a B_{12} cluster and one additional atom. This study[5] revealed that the redistribution of electron density within the unique polar-covalent 2e3c bond is the driving force for the observed charge separation in γ-B_{28}. Here we present an experimental electron-density study of α-B_{12} (Figs. 1 and 2) by single-crystal x-ray diffraction. We have found a 2e2c intercluster bond of similar nature as the 2e2c bond in γ-B_{28}.[5] A 2e3c bond is found that is different from the 2e3c bond in γ-B_{28}.[5] We show that the highly unusual arrangements of bond critical points (BCPs) within the intercluster 2e3c bond of α-B_{12} are indicative for the special arrangement of orbitals in the B_{12} cluster. Inspection of the experimental electron density of γ-B_{28} as published in Ref. 5 shows that it is in agreement with the same orbital order on B_{12} clusters. Together, these observations suggest that orbital order on B_{12} clusters might govern bonding in boron polymorphs and all boron-rich solids featuring this cluster.

II. EXPERIMENTAL

A. Measurement and data processing

High-quality single crystals of α-B_{12} were synthesized using the high-pressure high-temperature technique described elsewhere.[3] X-ray diffraction experiments were performed at beamline F1 of Hasylab, DESY, Hamburg, employing radiation of a wavelength of 0.5600 Å. A single crystal of

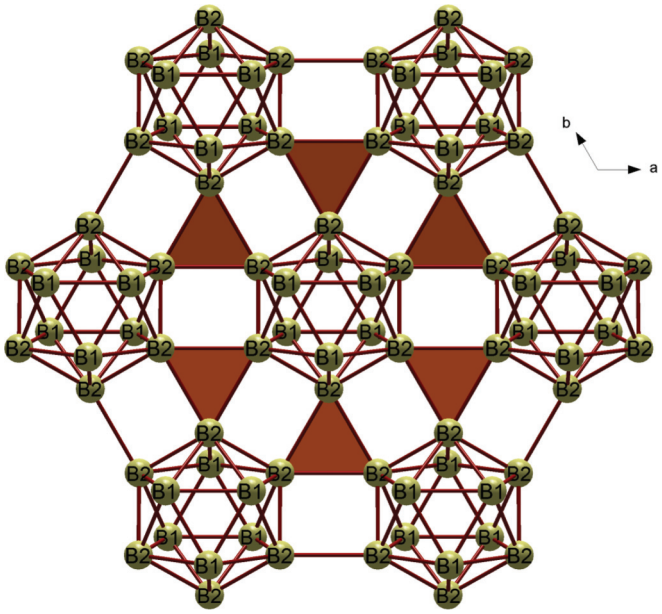

FIG. 1. (Color online) View of the crystal structure of α-B_{12} along the **c** axis. The crystallographically independent atoms B1 and B2 are indicated. The six inter-icosahedral 2e3c bonds of the central B_{12} cluster are highlighted in red color.

dimensions $0.07 \times 0.04 \times 0.03$ mm^3 was glued on a glass fiber attached to a copper pin and mounted on a Huber four-circle Kappa diffractometer equipped with a MARCCD area detector. The sample temperature was set by an open-flow nitrogen-gas cryostat. Diffraction images were obtained by ϕ and ω scans (1 degree rotation in 300 s exposure per image) for different offsets of the diffractometer angles. This resulted in a high redundancy and a complete data set up to $\sin(\theta)/\lambda = 1.221$ Å^{-1} (Table I). Indexing of Bragg reflections and extraction of integrated intensities from the diffraction images were performed with the software EVAL15.[19] This

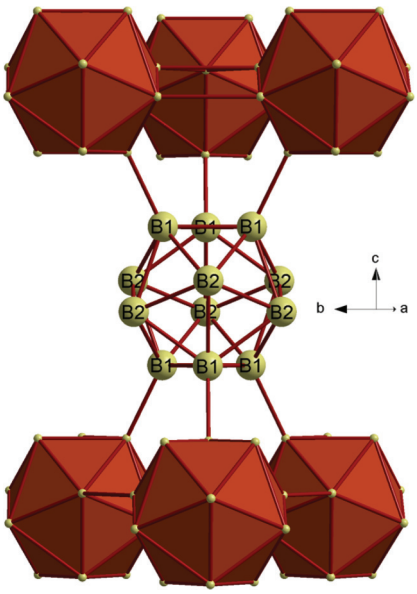

FIG. 2. (Color online) View of the crystal structure of α-B_{12} showing the six intercluster 2e2c bonds for the central B_{12} cluster.

TABLE I. Crystallographic data for α-B_{12}.

	Hasylab data		ESRF data
Crystal system	Trigonal		Trigonal
Space group	*R*-3*m*		*R*-3*m*
Z	36		36
a (Å)	4.9216(6)		4.9337(1)
c (Å)	12.6019(6)		12.6325(5)
Volume (Å^3)	264.35(5)		266.296(13)
F(000)	180		180
Temperature (K)	100		100
Wavelength, λ (Å)	0.5600		0.6980
$[\sin(\theta)/\lambda]_{max}$ (Å^{-1})	1.221		1.060
Observed criterion	$I > 3\sigma_I$		$I > 3\sigma_I$
No. of observed/all reflections	439/532		241/354
Multipole refinement	Hasylab data		ESRF data
$[\sin(\theta)/\lambda]_{max}$ (Å^{-1})	1.221	1.060[a]	1.060
R_F (obs)	0.0169	0.0116	0.0129
wR_F (obs)	0.0110	0.0092	0.0150
R_{F^2} (obs)	0.0191	0.0146	0.0179
wR_{F^2} (obs)	0.0220	0.0185	0.0306
GoF (obs)	1.6983	1.581	0.3843
$\triangle\rho_{max}$ (eÅ^{-3})	0.236	0.139	0.160
$\triangle\rho_{min}$ (eÅ^{-3})	−0.231	−0.150	−0.187

[a]Calculated with reflections up to 1.06 Å^{-1} after refinement against the full data set (first column).

software was also used for the application of a correction for the oblique effect. Approximately 3% of the reflections were rejected as outliers. The absorption correction, scaling and merging of equivalent reflections were done by the software SADABS.[20] The resulting data set is denoted as the Hasylab data (Table I).

A second diffraction experiment was conducted at beamline BM01A of the European Synchrotron Radiation Facility (ESRF), employing radiation of a wavelength of 0.6980 Å. A second crystal from the same batch and of dimensions $0.06 \times 0.05 \times 0.05$ mm^3 was glued to a glass fiber, and mounted on a KUMA6 diffractometer equipped with a SAPPHIRE CCD detector. Diffraction images were again acquired by ϕ and ω scans (1 degree rotation in 8 s or 16 s per image). Indexing and integration were now performed with CRYSALIS[21] software; scaling and the absorption correction were applied by SADABS,[22] while merging of equivalent Bragg reflections was done by SORTAV.[23] Approximately 6% of the measured reflections were removed as outliers. This data set is denoted as the ESRF data. The ESRF data set is of a lower resolution than the Hasylab data (Table I).

B. Multipole refinements

Initial coordinates of the crystallographically independent atoms were taken from our earlier work.[3] At first, a refinement according to the independent spherical atom model (IAM) was performed by SHELXL97.[24] The resulting structure model was introduced into the computer program XD2006[25] via the XDINI module. Subsequent refinements employed the multipole model of Hansen and Coppens[26] as implemented in the software package XD2006. In this model the electron density

TABLE II. Relative coordinates and ADPs (Å^2) of the crystallographically independent atoms in α-B_{12} as obtained by multipole refinement. Standard uncertainties are given in parentheses.

Parameter	B1	B2
x	0.118901 (22)	0.196900 (23)
y	−0.118901 (22)	−0.196900 (23)
z	−0.108666 (17)	0.024310 (17)
U_{11}	0.002500 (52)	0.002581 (52)
U_{22}	0.002500 (52)	0.002581 (52)
U_{33}	0.002056 (67)	0.002624 (71)
U_{12}	0.001455 (55)	0.001541 (55)
U_{13}	0.000135 (24)	−0.000039 (25)
U_{23}	−0.000135 (24)	0.000039 (25)

is written as the sum of electron densities of pseudoatoms, each of which consists of three terms:

$$\rho(\mathbf{r}) = \rho_{core}(r) + P_v \rho_{valence}(\kappa r) + \sum_l R_l(\kappa' r) \sum_{m=-l}^{l} P_{lm} y_{lm}\left(\frac{\mathbf{r}}{r}\right), \quad (1)$$

where, $\rho_{core}(r)$ and $\rho_{valence}(\kappa r)$ are the spherical core and valence electron densities. The third term corresponds to the deformation density. It consists of real, density-normalized spherical harmonics y_{lm} and the radial functions R_l. κ and κ' are screening constants, which account for expansion or contraction of the valence shell. P_v and P_{lm} are the refinable population parameters.

Each pseudoatom was assigned a neutral atom core, while core and valence scattering factors were taken from Su and Coppens.[27] Local coordinate systems for the spherical harmonics were individually chosen for both atoms on the basis of the crystallographic mirror plane. Only mirror symmetric multipoles expanded up to hexadecapole ($l = 4$) were refined in the final model. Both radial expansion and contraction parameters (κ and κ') for crystallographically independent atoms were refined. The function minimized in the least-squares refinements is $\sum w(|F_o| - k|F_c|)^2$ for reflections with $I > 3\sigma_I$, and with a weight of $w = \frac{1}{\sigma^2(F_o)}$.

The final multipole model (Table II) yields an excellent fit to the Hasylab data (Table I). An almost featureless residual density map (Figs. 3 and 4) confirms that all density is described by this model. Two-dimensional (2D) contour maps of electron densities and their gradient trajectories from the final model were prepared using the XDGRAPH[25] module of the XD2006 software package. Isosurface plots were generated by the computer program MOLISO.[28]

Integrated properties and topological properties according to Bader's quantum theory of atoms in molecules (AIM)[29] were obtained for the static electron density corresponding to the final multipole model with aid of the module XDPROP[25] of the XD2006 software package. The AIM theory states that bonding interactions between atoms require the presence of a BCP and/or ring critical point (RCP) in the electron density at a location between those atoms. Values of the electron density and its Laplacian at BCPs and RCPs characterize the nature of a bond (Table III). Charges of atoms are obtained by integration of the electron density of the atomic basins (Table IV).

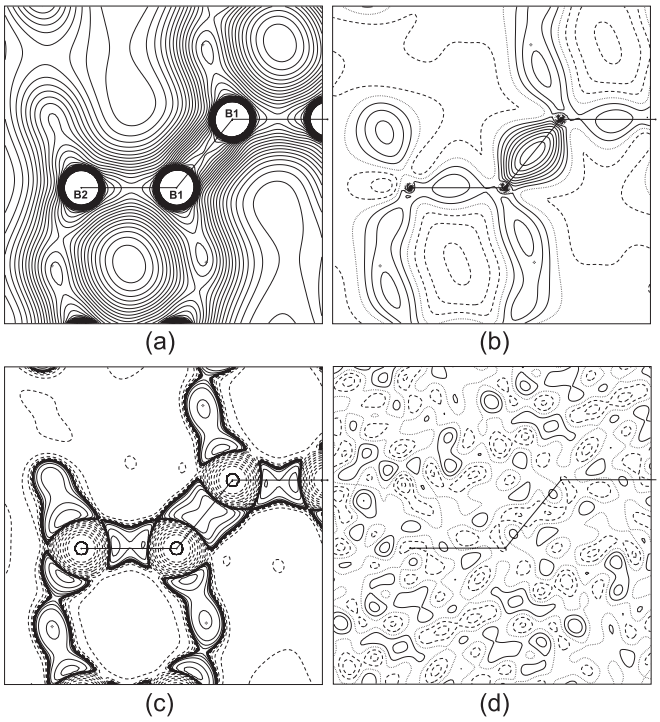

FIG. 3. Sections of 6 × 6 Å^2 centered on the B2–B1–B1 atoms, containing the B1–B1 intercluster 2e2c bond in α-B_{12}. (a) Electron density; contour lines at intervals of 0.05 up to 2.0 electron Å^{-3}. (b) Deformation density; contours at 0.05 electron Å^{-3}. (c) Laplacian; contours at $\pm(2, 4, 8)\times 10^n$ electron Å^{-5} ($-3 \leqslant n \leqslant 3$). (d) Residual density calculated with data up to $\sin(\theta)/\lambda = 1.06$ Å^{-1}; contours at 0.05 electron Å^{-3}. Solid contour lines are for positive values, dashed lines for negative values, and dotted lines for the zero contour.

A second multipole refinement has been independently carried out against the ESRF data, employing the same strategy (Table I). Exactly the same set of critical points with similar values of electron densities and Laplacians has been found for the static electron densities obtained from either refinement, confirming the present model. However, the ESRF data are of lower resolution as compared to the Hasylab data (Table I).

TABLE III. Topological properties of the static electron density from the multipole model of α-B_{12}. r_{bcp} are the distances between the atoms and the BCP in a bond.

Bond	r_{bcp} (Å)	ρ (eÅ^{-3})	$\nabla^2\rho$ (eÅ^{-5})
	Intra-icosahedral interactions		
B1–B1	0.890, 0.890	0.820	−2.258
B1–B2	0.865, 0.946	0.745	−1.388
B1–B2	0.858, 0.945	0.764	−1.950
B2–B2	0.894, 0.894	0.804	−2.470
B2–B1–B1		0.704	−1.955
B1–B2–B2		0.716	−4.321
B1–B1–B1		0.795	−1.155
	Inter-icosahedral interactions		
B1–B1	0.837, 0.837	1.104	−9.572
B2–B2	1.080, 1.080	0.561	−1.239
B2–B2–B2		0.557	−1.063
B2–B2–B2–B2		0.239	2.104

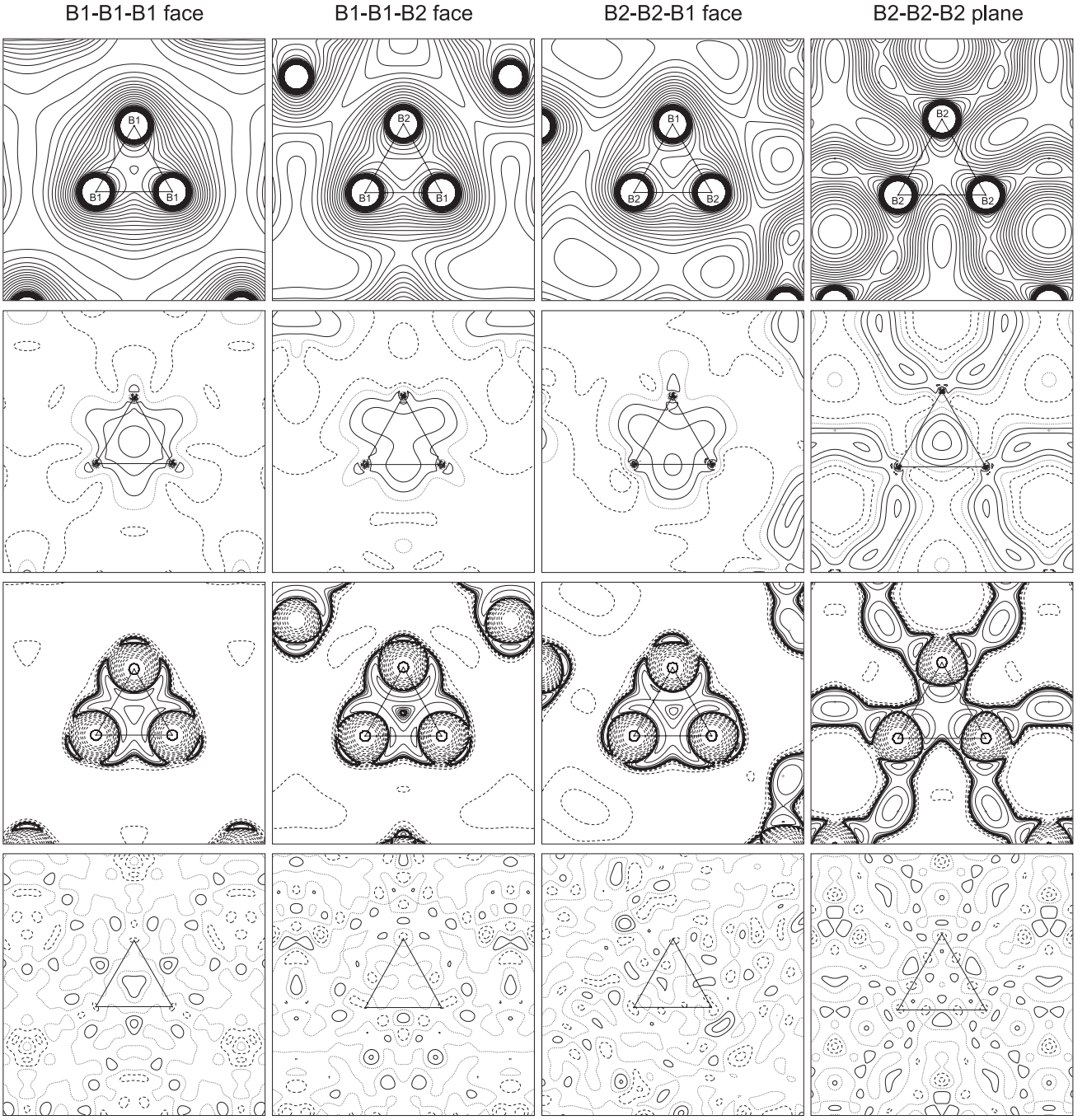

FIG. 4. Sections of 6×6 Å^2 of the multipole electron density of α-B_{12}. Four different planes are shown as indicated at the top of each column. First row: electron density; contour lines at intervals of 0.05 up to 2.0 electron Å^{-3}. Second row: deformation density; contours at 0.05 electron Å^{-3}. Third row: Laplacian; contours at $\pm(2, 4, 8)\times 10^n$ electron Å^{-5} ($-3 \leqslant n \leqslant 3$). Fourth row: Residual density calculated with data up to $\sin(\theta)/\lambda = 1.06$ Å^{-1}; contours at 0.05 electron Å^{-3}. Solid contour lines are for positive values, dashed lines for negative values, and dotted lines for the zero contour.

Furthermore, the latter data are of higher quality, as is evident from the values of partial R factors calculated for a subset of the reflections from the Hasylab data, which corresponds to the available reflections in the ESRF data set. The partial R values for the Hasylab data are lower than the R values for refinement against the ESRF data (Table I). The better quality of the Hasylab data is also evident from the structure models, e.g., with standard uncertainties of atomic coordinates and atomic displacement parameters (ADPs) being approximately twice as low in case of the refinement against the Hasylab data than for refinement against ESRF data. Reasons behind these differences might be a lower quality of the crystal used for the data collection at the ESRF and/or the differences in the data collection and data processing procedures. Since the quality and the resolution of the Hasylab data have been found to be better than those of the ESRF data (Table I), we

TABLE IV. Bader charges for the atoms in α-B_{12} (this work) and γ-B_{28} (Ref. 5).

γ-B_{28}		α-B_{12}	
Atom	Charge	Atom	Charge
B1	+0.0571	B1	+0.0668
B2	−0.1386	B2	−0.0674
B3	+0.0011		
B4	−0.1943		
B5	+0.4138		

have restricted the discussion to the results obtained with the Hasylab data.

C. Calculations according to the maximum entropy method

An electron-density study without the multipole model is possible with the maximum entropy method (MEM) applied to x-ray diffraction data. An accurate description of the electron density in the neighborhood of critical points requires a prior or reference electron density that is close to the final density.[30,31] For many years, the electron density corresponding to the IAM has been used for this purpose. Recently, we have shown that the use of a prior electron density calculated from an IAM obtained by strategic refinement against high-order data (IAM-HO electron density) produces better MEM electron densities than the IAM prior.[32]

Following this finding, a strategic refinement was performed against the high-order reflections [$\sin(\theta/\lambda) > 0.70$ Å^{-1}] of the Hasylab data, using the computer program XD2006.[25] This refinement resulted in the IAM-HO model. The IAM-HO electron density was then computed with the computer program PRIOR.[30,33] The computer program BAYMEM[30] was used for MEM calculations, employing the IAM-HO electron density as prior.[32] Electron densities were described on a grid of 132 × 132 × 324 pixels over the unit cell, which corresponds to a grid spacing of ∼ 0.04 Å. Twelve different MEM calculations were performed with different χ^2_{aim} values in the range of 0.75 to 2.0. The final choice of $\chi^2_{aim} = 1.60$ and the choice of the weighting scheme $H4$ were made according to procedures discussed elsewhere.[32,34–36] 2D contour maps were plotted using the program JANA2006.[37]

III. DISCUSSION

The structure of α-B_{12} can be described as a distorted cubic closest packing of icosahedral B_{12} clusters as "spheres." Each B_{12} cluster is connected to six neighboring B_{12} units by three-center (3c) bonds within the same close-packed layer perpendicular to the threefold symmetry axis (Fig. 1). Each cluster is furthermore connected to three B_{12} clusters within the layer above and three clusters within the layer below through two-center (2c) bonds (Fig. 2). Chemical bonding in α-B_{12} obeys the Wade-Jemmis rules[11–13] for *closo*-clusters as follows.[7,38,39] The B_{12} cluster has 36 valence electrons; 26 of them are used to form the B_{12} *closo*-cluster.[11–13] Six more valence electrons are used to form six 2e2c inter-cluster bonds (Fig. 2). The remaining four electrons are involved in six intercluster 2e3c bonds as indicated in Fig. 1.

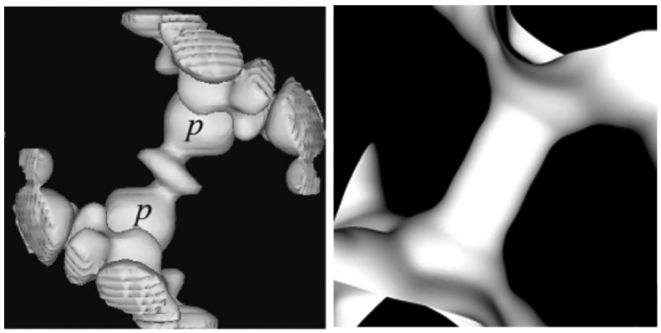

FIG. 5. Isosurface plots of electron densities of α-B_{12}, showing the region about the intercluster 2e2c bond. Left: reproduced with permission from Hosoi *et al.* (2007) (Ref. 39). Right: from the multipole model of the present study. The isosurface level is 0.69 electron Å^{-3}.

Icosahedral boron-rich solids are sometimes denoted as inverted molecular solids due to the fact that inter-icosahedral bonds in these solids are stronger than or at least as strong as those within the icosahedral cluster.[40] From the topological analysis of the electron density of α-B_{12} (Table III), we have found that the intercluster 2e2c B1–B1 bond is the strongest bond since it has the highest magnitudes of electron density (ρ_{BCP}) and Laplacian ($\nabla^2\rho_{BCP}$) at its BCP among all bonds. On the basis of a qualitative electron-density analysis by the MEM applied to powder x-ray diffraction data, Fujimori *et al.* (1999)[7] and Hosoi *et al.* (2007)[39] have suggested that the inter-icosahedral 2e2c bond is bent. An isosurface plot (Fig. 5) reveals no unusual (bent) feature unlike that reported by Hosoi *et al.* (2007).[39] Static electron densities, deformation densities, and Laplacians plotted on the B2–B1–B1 plane (Fig. 3) reveal the strong character of the B1–B1 bond, but do not indicate any unusual distribution of electron density or bent nature of the bond. The present MEM-electron density, obtained by the MEM applied to the present single-crystal x-ray diffraction data (Sec. II C), is similar to the electron density of the multipole model and does not exhibit any bent character either (Fig. 6). The peculiar electron-density distribution reported earlier[7,39] for this bond thus seems to be an artifact caused by the limited information content of the powder diffraction data.

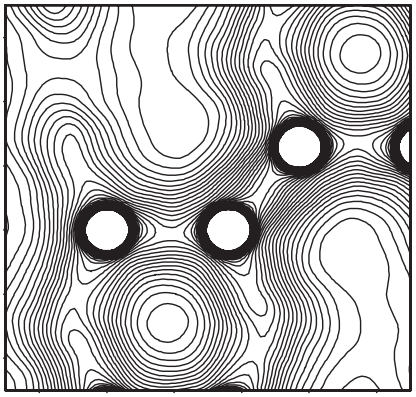

FIG. 6. The MEM-electron density of α-B_{12}. The same plane is shown as in Fig. 3. Contours are drawn at intervals of 0.05 up to 2.5 electron Å^{-3}.

The topological analysis (Table III) reveals ring critical points (RCPs) for all faces of the icosahedral cluster and BCPs for all constituent 2c interactions. Together they imply multicenter bonds on the B_{12} *closo*-cluster. Static deformation densities and Laplacians in the faces of the B_{12} icosahedral cluster in α-B_{12} have similar appearances as corresponding maps for dodecaboranes ($[B_{12}H_{12}]^{2-}$ molecular anions).[41] Values of the electron density at the BCPs and RCPs of these faces match well with the values of electron densities of B_{12} clusters in dodecaboranes[41] and in γ-B_{28}.[5] However, magnitudes of Laplacians at RCPs of these faces are larger than corresponding quantities of the B_{12} cluster in both the dodecaboranes[41] and γ-B_{28}.[5] Unlike γ-B_{28}, no positive Laplacian at RCPs on these faces have been observed in α-B_{12}.

The static electron density, the deformation density and the Laplacian clearly show that inter-icosahedral 2e3c bond (B2–B2–B2 plane) is different from the B1–B1–B2 and B2–B2–B1 faces that are part of the molecular-orbital-type of bond on the B_{12} cluster (Fig. 4). At first glance, the B1–B1–B1 face of the B_{12} cluster appears similar to the 2e3c bond on B2–B2–B2: both exhibit threefold symmetry. However, a closer look, especially on the Laplacian maps, reveals significant differences. The value of electron density at the RCP of the exocluster 2e3c bond is the lowest among all 3c interactions (Table III). This value is similar to the value obtained for the 2e3c bond in γ-B_{28}.[5] The Laplacian at the RCP for the B2–B2–B2 bond is negative, in agreement with a covalent character of this bond. In case of γ-B_{28}, the Laplacian at the RCP of the 2e3c bond has a positive value, indicating its polar-covalent character.[5]

In our previous study[5] on γ-B_{28}, we have found a significant amount of charge transfer between boron atoms, in agreement with theory.[4] Fujimori *et al.* (1999)[7] proposed charge transfer in α-B_{12}. First-principles calculations of the electronic structure suggested significant ionicities[6] of the B–B bonds in α-B_{12}. Presently, we have obtained atomic charges of the two crystallographically independent atoms in α-B_{12} by integration over the atomic basins of the static electron density (Table IV). Neither ionicity[6] nor a charge transfer (like in γ-B_{28})[5] are found for α-B_{12}. We also noticed that a charge separation for the exocluster 2e3c bond is forbidden by the threefold symmetry of α-B_{12}.

Molecular orbital calculations[8,10] using four valence orbitals for each boron atom of the B_{12} cluster have obtained 13 molecular-orbital-type bonding orbitals on the cluster, 23 antibonding orbitals, and 12 bonding orbitals perpendicular to the surface of the cluster. Unsurprisingly, the directions of these 12 bonding orbitals are in complete agreement with the formation of 12 equivalent B–H bonds of $[B_{12}H_{12}]^{2-}$ molecular anions in dodecaboranes.[41] However, the orbital order of the 12 external bonding orbitals of the B_{12} cluster persists in the highly asymmetric external bonding of this cluster in γ-B_{28} and α-B_{12}. The orbital order is obvious for the 2e2c and 1e2c intercluster bonds, whose bond paths are perpendicular to the surface of the B_{12} clusters (Figs. 3 and 7), and thus are in agreement with the directions of the external bonding orbitals of the free B_{12} cluster. The unusual arrangements of BCPs within the intercluster 2e3c bonds are also explained by the proposed orbital order on the B_{12} clusters. In case of α-B_{12}, BCPs are very close to the central RCP of the 3c ring and the bond paths are heavily bent inward [Fig. 7(a)]. In case of γ-B_{28}, opposite features, i.e., outward bent bond paths, are found in the electron density map [Fig. 7(b)].[5] However, in both cases, bond paths are perpendicular to the surface of the B_{12} cluster near the atoms defining the 2e3c bonds, in agreement with the proposed orbital order. In case of α-B_{12}, three orbitals from the three different B_{12} clusters overlap at the center of the threefold ring, thus explaining the inward bending of the bond paths. The same conclusion can be drawn on the bent bond paths in case of γ-B_{28}, now leading to outward bending of the bond paths. Isosurface plots (Fig. 8) show lobes of high electron density in directions perpendicular to the surface of the B_{12} clusters, again in agreement with the proposed orbital order. It is thus found that orbital order of the free B_{12} cluster persists for this cluster in α-B_{12}, γ-B_{28}, and several dodecaboranes,[41] irrespective of the fact that these clusters participate in entirely different kinds of intercluster bonds.

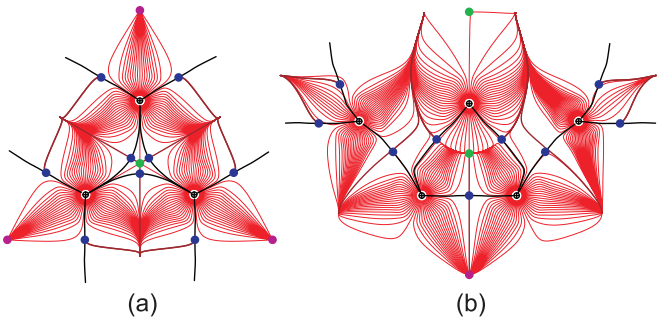

FIG. 7. (Color online) Gradient trajectories of the electron densities. (a) 2e3c bond in α-B_{12}. (b) 2e3c bond in γ-B_{28} [adapted from Fig. 3(c) in Mondal *et al.* (2011) (Ref. 5)]. Bond paths are drawn as thick black lines. BCPs and RCPs are drawn in blue and green colors respectively.

A particular exocluster B–B bond has been proposed for γ-B_{28} on the basis of electronic-structure calculations and the relatively short bond length of 2.086 Å.[4,42] Its existence was refuted in our previous work on the basis of the absence of a BCP between these atoms in the experimental electron density.[5] The observation of the orbital order on B_{12} clusters explains the absence of this bond, despite the close proximity of the corresponding atoms, as the result of an unfavorable orientation of the external bonding orbitals of the B_{12} cluster.

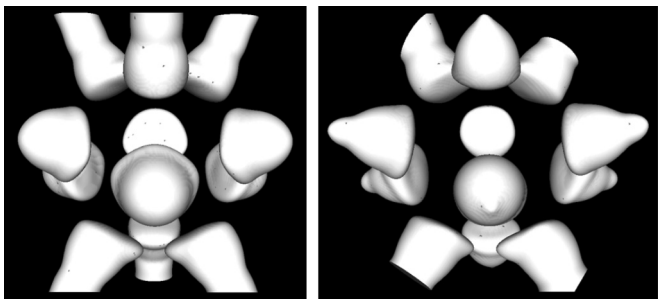

FIG. 8. Isosurface plots of electron densities about the B_{12} cluster. Left: in α-B_{12}; right: in γ-B_{28}. The plotted surface corresponds to the density of 0.84 electron Å^{-3}. They demonstrate the proposed orbital order by lobes of high densities perpendicular to the surfaces of the clusters.

These observations strongly suggest that, in solids containing B_{12} clusters, chemical bonding is governed by the directions of bonding orbitals on the B_{12} cluster rather than by the proximities of atoms.

IV. CONCLUSIONS

An accurate experimental electron density of α-B_{12} has been obtained on the basis of a multipole refinement against low-temperature single-crystal x-ray diffraction data measured on a high-quality single crystal. A quantitative analysis of the topological properties of this electron density has shown that the intercluster 2e2c bond is the strongest bond in α-B_{12}, in agreement with the finding of a strong 2e2c intercluster bond in γ-B_{28}.[5] No unusual (bent) features of this bond have been found in the static multipole density nor in the MEM-electron density, contrary to previous work based on powder x-ray diffraction data.[7,39]

The bent character of bond paths and the unusual arrangements of BCPs for the exo-cluster 2e3c bonds in both α-B_{12} and γ-B_{28} (Ref. 5) are explained by orbital order on the B_{12} clusters. All exocluster bonding of the B_{12} clusters is governed by one orbital per boron atom that is oriented perpendicular to the surface of the B_{12} clusters. It is argued that a previously proposed[4,42] exocluster B–B bond in γ-B_{28} cannot exist due to an unfavorable orientation of the external bonding orbitals of the B_{12} cluster. Unlike γ-B_{28}, a significant charge separation between boron atoms could not be found in α-B_{12}.

Orbital order of the 12 external bonding orbitals on the B_{12} cluster is found to persist in two boron polymorphs and several dodecaboranes,[41] despite the fact that these clusters participate in entirely different kinds of exocluster bonds. It is likely that the same orbital order of B_{12} clusters can explain bonding in other boron polymorphs and boron-rich solids.

ACKNOWLEDGMENTS

Financial support has been obtained from the German Science Foundation (DFG). N.D. thanks the DFG for financial support through the Heisenberg program.

*smash@uni-bayreuth.de

[1] B. Albert and H. Hillebrecht, Angew. Chem. **121**, 8794 (2009).
[2] E. Yu. Zarechnaya, L. Dubrovinsky, N. Dubrovinskaia, Y. Filinchuk, D. Chernyshov, V. Dmitriev, N. Miyajima, A. El Goresy, H. F. Braun, S. Van Smaalen, I. Kantor, A. Kantor, V. Prakapenka, M. Hanfland, A. S. Mikhaylushkin, I. A. Abrikosov, and S. I. Simak, Phys. Rev. Lett. **102**, 185501 (2009).
[3] G. Parakhonskiy, N. Dubrovinskaia, L. Dubrovinsky, S. Mondal, and S. van Smaalen, J. Cryst. Growth **321**, 162 (2011).
[4] A. R. Oganov, J. H. Chen, C. Gatti, Y. Z. Ma, Y. M. Ma, C. W. Glass, Z. X. Liu, T. Yu, O. O. Kurakevych, and V. L. Solozhenko, Nature (London) **457**, 863 (2009).
[5] S. Mondal, S. van Smaalen, A. Schönleber, Y. Filinchuk, D. Chernyshov, S. I. Simak, A. S. Mikhaylushkin, I. A. Abrikosov, E. Zarechnaya, L. Dubrovinsky, and N. Dubrovinskaia, Phys. Rev. Lett. **106**, 215502 (2011).
[6] J. He, E. Wu, H. Wang, R. Liu, and Y. Tian, Phys. Rev. Lett. **94**, 015504 (2005).
[7] M. Fujimori, T. Nakata, T. Nakayama, E. Nishibori, K. Kimura, M. Takata, and M. Sakata, Phys. Rev. Lett. **82**, 4452 (1999).
[8] H. C. Longuet-Higgins and M. de V. Roberts, Proc. R. Soc. London A **230**, 110 (1955).
[9] W. N. Lipscomb and D. Britton, J. Chem. Phys. **33**, 275 (1960).
[10] D. W. Bullet, in *Boron-rich Solids*, edited by D. Emin, T. Aselage, C. L. Beckel, I. A. Howard, and C. Woods, AIP Conf. Proc. No. 140 (AIP, New York, 1986), pp. 249–259.
[11] K. Wade, J. Chem. Soc. Chem. Commun. 792 (1971).
[12] K. Wade, Adv. Inorg. Chem. Radiochem. **18**, 1 (1976).
[13] E. D. Jemmis, M. M. Balakrishnarajan, and P. D. Pancharatna, J. Am. Chem. Soc. **123**, 4313 (2001).
[14] L. V. McCarty, J. S. Kasper, F. H. Horn, B. F. Decker, and A. E. Newkirk, J. Am. Chem. Soc. **80**, 2592 (1958).
[15] D. E. Sands and J. L. Hoard, J. Am. Chem. Soc. **79**, 5582 (1957).
[16] R. E. Hughes, C. H. L. Kennard, D. B. Sullenger, H. A. Weakliem, D. E. Sands, and J. L. Hoard, J. Am. Chem. Soc. **85**, 361 (1963).
[17] C. P. Talley, S. La Placa, and B. Post, Acta Crystallogr. **13**, 271 (1960).
[18] M. Vlasse, R. Naslain, J. S. Kasper, and K. Ploog, J. Solid State Chem. **28**, 289 (1979).
[19] A. M. M. Schreurs, X. Xian, and L. M. J. Kroon-Batenburg, J. Appl. Crystallogr. **43**, 70 (2010).
[20] G. M. Sheldrick, SADABS 2008/1, Bruker AXS Inst. Inc., Madison, Wisconsin, USA.
[21] CRYSALIS Software System, Ver. 1.171.33.55, 2009, Oxford-diffraction Ltd., Oxford, UK.
[22] G. M. Sheldrick, SADABS, Ver. 2.06, 2002, Empirical Absorption Correction Program, University of Göttingen, Germany.
[23] R. H. Blessing, J. Appl. Crystallogr. **30**, 421 (1997).
[24] G. M. Sheldrick, Acta Crystallogr. Sect. A **64**, 112 (2008).
[25] A. Volkov, P. Macchi, L. J. Farrugia, C. Gatti, P. R. Mallinson, T. Richter, and T. Koritsanszky (2006), computer program XD2006, http://xd.chem.buffalo.edu/.
[26] N. K. Hansen and P. Coppens, Acta Crystallogr. Sect. A **34**, 909 (1978).
[27] Z. Su and P. Coppens, Acta Crystallogr. Sect. A **54**, 646 (1998).
[28] C. B. Hübschle and P. Luger, J. Appl. Crystallogr. **39**, 901 (2006).
[29] R. F. W. Bader, *Atoms in Molecules-A Quantum Theory* (Oxford University Press, New York, 1990).
[30] S. van Smaalen, L. Palatinus, and M. Schneider, Acta Crystallogr. Sect. A **59**, 459 (2003).
[31] M. Takata, Acta Crystallogr. Sect. A **64**, 232 (2008).
[32] S. J. Prathapa, S. Mondal, and S. van Smaalen, Acta Crystallogr. Sect. B **69**, 203 (2013).
[33] S. Mondal, S. J. Prathapa, and S. van Smaalen, Acta Crystallogr. Sect. A **68**, 568 (2012).
[34] A. Hofmann, J. Netzel, and S. van Smaalen, Acta Crystallogr. Sect. B **63**, 285 (2007).
[35] A. Hofmann, R. Kalinowski, P. Luger, and S. van Smaalen, Acta Crystallogr. Sect. B **63**, 633 (2007).
[36] J. Netzel, A. Hofmann, and S. van Smaalen, CrystEngComm **10**, 335 (2008).

[37]V. Petricek, M. Dusek, and L. Palatinus, JANA2006 crystallographic computing system, Institute of Physics, Czech Academy of Sciences, Praha, Czech Republic.
[38]G. Will and B. Kiefer, Z. Anorg. Allg. Chem. **627**, 2100 (2001).
[39]S. Hosoi, H. Kim, T. Nagata, K. Kirihara, K. Soga, K. Kimura, K. Kato, and M. Takata, J. Phys. Soc. Jpn. **76**, 044602 (2007).
[40]D. Emin, Phys. Today **40**(1), 55 (1987).
[41]S. Mebs, R. Kalinowski, S. Grabowsky, D. Forster, R. Kickbusch, E. Justus, W. Morgenroth, C. Paulmann, P. Luger, D. Gabel, and D. Lentz, Inorg. Chem. **50**, 90 (2011).
[42]P. Rulis, L. Wang, and W. Y. Ching, Phys. Status Solidi R **3**, 133 (2009).